Search for Manifestation of Strong Coupling as Critical Point of Fine Particle Plasmas in PK-3 PLUS

Hiroo TOTSUJI [*1], Kazuo TAKAHASHI [*2], and Satoshi ADACHI [*3]

Abstract: The fine particle (dusty) plasma is a charge-neutral mixture of micron-sized fine (dust) particles and ambient plasma composed of ions and electrons. Typical densities of fine particles and ambient plasmas are $(10^4 \sim 10^5)$ cm^{-3} and $(10^6 \sim 10^8)$ cm^{-3}, respectively. Images of fine particles are easily captured and identified by CCD cameras through the scattering of the laser beam and we are able to make particle level observations. In contrast to singly charged ions or electrons, fine particles in plasmas have large negative charges up to 10^3 or even 10^4 times as large as that of an electron, enabling observations of various effects coming from the strong Coulomb coupling between fine particles. For this reason, a lot of researches on fine particle plasmas have been performed recently. One of the most interesting phenomena in strongly coupled systems may be the ones related to the critical point. In this report, we give a summary of our proposal to observe critical phenomena in fine particle plasmas in PK-3PLUS under the condition of the microgravity and the present status of data analysis. In Part I, the theoretical background is given and the possibility to observe the critical point is shown with an emphasis on the difference between the simple one-component plasma (OCP) model of the charged particle systems and systems with the background as real physical entity. In Part II, characteristic parameters realized in PK-3 PLUS are analyzed in relation to those of the critical point. The behavior of the structure factor is discussed in comparison with the effects of inhomogeneity and finiteness of observed samples and conclusions are given.

Keywords: Fine Particle Plasmas, Strong Coupling, Critical Point, PK-3 Plus, Microgravity, ISS

Part I: Theoretical Background

1. One-component plasma (OCP) model

Macroscopic systems of charged particles are usually almost charge neutral including almost the same number of positive and negative charges. In theoretical treatment, however, it is useful to mainly consider only one component. In this case, systems of charged particles are called one-component plasma (OCP). An example of the classical OCP is atomic nuclei in degenerate electrons (the Fermi sea) and that of the degenerate (quantum) OCP is the electron liquid in positively charged jellium. In OCP, the disregarded components which guarantee the charge neutrality of the system are called *background*. It should be noted that, *from the definition of the OCP model, the background has no contribution to physical quantities of the system such as pressure*.

In addition to the neutralization, the background can be considered to be polarizable and, in the case of Debye-Hückel screening, we have the Yukawa OCP. The system of fine (dust) particles in fine particle plasmas (dusty plasmas), charge-neutral mixtures of macroscopic fine particles (dust particles) and ambient plasma of ions and electrons, is one of typical examples for which the Yukawa system is considered to be a model in the first approximation [1–4].

It has been pointed out that fine particle plasmas possibly manifest critical behavior [5–10]. Previously, the existence of the attraction between particles was assumed as the essential requirement for such behavior [5] or the mean field analysis on the Yukawa system was given [6]. Based on the intrinsic tendency of the OCP to become thermodynamically unstable with the increase of the Coulomb coupling [7], we have shown that there appears the critical point when particles are very strongly coupled, taking the deformation of the background plasma explicitly into account [8–10]. Though this condition is not easy to realize in usual experiments, the Yukawa particles in ambient plasma can provide us a possibility of observation of critical behavior at the kinetic level. The only weakness of the system is the effect of the gravity which is inevitable for macroscopic particles necessary for very strong

*1 Okayama University, 3-1-1 Tsushimanaka, Kitaku, Okayama 700-8530, Japan
*2 Department of Electronics, Kyoto Institute of Technology, Matsugasaki, Sakyo-ku, Kyoto 606-8585, Japan
*3 Institute of Space and Astronautical Science, Japan Aerospace Exploration Agency, 2-1-1 Sengen, Tsukuba, Ibaraki 305-8505, Japan
(E-mail: totsuji-09@t.okadai.jp)

This document is provided by JAXA.

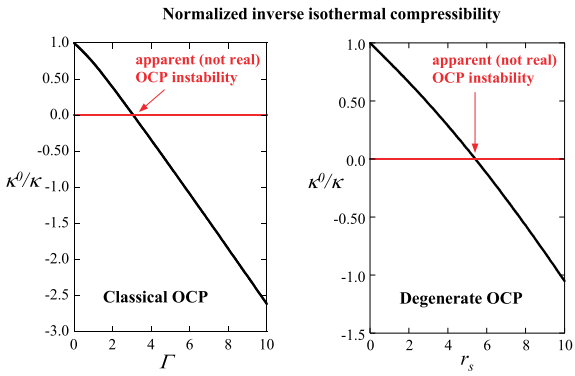

Fig. 1 Inverse isothermal compressibility of one-component plasmas $1/\kappa$ normalized by the ideal gas value $1/\kappa^0$. Classical OCP (left), and degenerate OCP (right). In both cases, the isothermal compressibility has an apparent divergence. In real systems, the contribution of the background should be taken into account.

strong coupling. Therefore fine particle plasmas realized in PK-3 PLUS in the microgravity environment have a possibility to give experimental verification of such phenomena[11].

2. Pressure and isothermal compressibility of OCP

The pressure is given by the volume derivative of the Helmholtz free energy at constant temperature. Within the OCP model, the neutralizing background does not contribute to the pressure of the system: It is assumed to deform automatically *without work* in the process of changing the volume[12].

When the coupling is sufficiently strong, the internal energy of OCP becomes negative due to the negative non-ideal part. The pressure of OCP also becomes negative: This is due to the virial theorem in the case of OCP with pure Coulomb interaction[13] and this occurs also for the Yukawa OCP[8]. Along with the pressure, the inverse isothermal compressibility of the OCP also becomes negative when the coupling becomes strong[8–10,14]. Examples of classical and degenerate pure Coulomb OCP's are shown in Fig. 1 where the coupling in the classical case is expressed by dimensionless parameters $\Gamma = (4\pi n/3)^{1/3} e^2/k_B T$ and, in the degenerate case, by $r_s = (3/4\pi n)^{1/3}/a_B$, n, e, T, and a_B being the number density, the charge, and the temperature and the Bohr radius, respectively.

In contrast to ordinary systems where vanishing of the inverse isothermal compressibility means a thermodynamic instability, vanishing inverse isothermal compressibility does not directly mean such an instability in the case of OCP. In the rigid background, for example, nothing peculiar happens even if the inverse isothermal compressibility of OCP vanishes[14]. The necessity of the background deformation for the observation of the instability has been shown by evaluating the deformation spectrum of the background near the vanishing point of the inverse isothermal compressibility[7].

For real systems, we have to explicitly specify the background. If not completely rigid, the background in systems modeled as OCP has its own pressure which is usually high enough to mask the intrinsic thermodynamic instability of the OCP. In fine particle plasmas, the background plasma is classical and *the Yukawa particles are in polarizing and neutralizing ambient plasma which is deformable in principle*. When the Yukawa particles are sufficiently strongly coupled, their negative contribution to the inverse isothermal compressibility can overcomes the positive contribution from the ambient background plasma. The divergence of the isothermal compressibility of the total system means a thermodynamic instability and density fluctuations are enhanced when we approach to this instability[7]. When the condition of the instability is attained, we may have a transition to a state composed of phases with different densities. We thus expect the existence of the critical point.

3. Yukawa particles in polarizing and neutralizing ambient plasma

Let us consider the system in a volume V composed of N_e electrons with the charge $-e$, N_i ions with the charge e, and N_p particles with the charge $-Qe$, satisfying the charge neutrality

$$(-e)N_e + eN_i + (-Qe)N_p = 0. \tag{1}$$

For densities of electrons, ions, and particles, $n_e = N_e/V$, $n_i = N_i/V$, and $n_p = N_p/V$, we assume n_i, $n_e \gg n_p$ and take the statistical average with respect to electrons and ions to obtain the Helmholtz free energy of the system in the form[15,16]

$$\begin{aligned} F =& F_{id}^{(e)}(T_e, V, N_e) + F_{id}^{(i)}(T_i, V, N_i) \\ &+ F^{(p)}(T_p, V, N_p), \end{aligned} \tag{2}$$

This document is provided by JAXA.

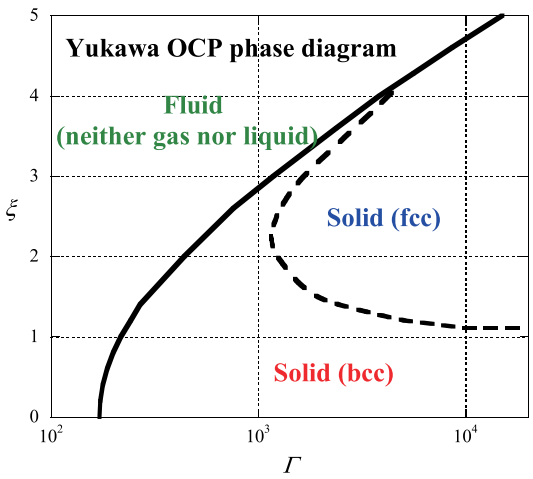

Fig. 2 Phase diagram of Yukawa OCP.

where

$$F^{(p)}(T_p,V,N_p) = -k_B T_p \ln\left[\frac{1}{(2\pi\hbar)^{3N_p}N_p!}\times \iint_V \prod_{i=1}^{N_p} d\mathbf{r}_i d\mathbf{p}_i \exp[-(K_p+U_p)/k_B T_p]\right]. \quad (3)$$

The terms $F_{id}^{(e)}$ and $F_{id}^{(i)}$ are the ideal gas contribution from electrons and ions at temperatures T_e, and T_i, respectively. The term $F^{(p)}$ is the contribution from particles at the temperature T_p where K_p is the kinetic energy of particles and U_p is the Helmholtz free energy for given configuration of particles, $\{\mathbf{r}_i\}_{i=1,2,\ldots N_p}$. We assign different temperatures to particles and ambient microscopic particles.

When we neglect the electron-electron, electron-ion, and ion-ion correlation and regard particles as points, U_p in Eq. (3) is given by a sum of the cohesive energy U_{coh} and the energy associated with the sheath U_{sheath} [15)]

$$U_p = U_{coh} + U_{sheath}, \quad (4)$$

where

$$U_{coh} = \frac{1}{2}\sum_{i\neq j}^{N_p}\frac{(Qe)^2}{r_{ij}}\exp(-r_{ij}/\lambda) - N_p\frac{n_p}{2}\int d\mathbf{r}\frac{(Qe)^2}{r}\exp(-r/\lambda), \quad (5)$$

$$U_{sheath} = -\frac{N_p}{2}\frac{(Qe)^2}{\lambda}, \quad (6)$$

and

$$\frac{1}{\lambda^2} = \frac{4\pi n_e e^2}{k_B T_e} + \frac{4\pi n_i e^2}{k_B T_i}. \quad (7)$$

As indicated by the first term on the right hand side of Eq. (5), the interaction between particles is the repulsive Yukawa potential. Note that, when there is no correlation between particles, $U_{coh} = 0$ due to the second term. Particles develop mutual correlation to reduce U_{coh} to $U_{coh} < 0$ from the uncorrelated value $U_{coh} = 0$. In other words, particles not only interact via the repulsive Yukawa potential but also are *effectively confined* by the second term of Eq. (5) due to the charge neutrality of the whole system [15)]. Though one is tempted to consider that some confining force is necessary to keep repulsive Yukawa particles in a finite volume, charge neutral systems are basically self-confined.

The system of point particles interacting via the Yukawa repulsive potential $(Qe)^2\exp(-r/\lambda)/r$ is called Yukawa one-component plasma (Yukawa OCP) and its static and dynamic properties have been obtained extensively by various methods including numerical simulations [17–19)]. The Yukawa OCP is characterized by the parameters Γ and ξ defined respectively by

$$\Gamma = \frac{(Qe)^2}{ak_B T_p} \quad (8)$$

and

$$\xi = \frac{a}{\lambda}, \quad (9)$$

$a = (3/4\pi n_p)^{1/3}$ being the mean distance between particles. The phase diagram is shown in Fig. 2.

The energy associated with correlation between particles is given by

$$\frac{n_p}{2}\int d\mathbf{r}\frac{(Qe)^2}{r}\exp(-r/\lambda)[g(r)-1], \quad (10)$$

$g(r)$ and $g(r)-1$ being the pair distribution and the pair correlation functions, respectively. We note that this energy (usually called 'internal energy') is nothing but the statistical average of U_{coh}: -1 in [ ] in Eq. (10) corresponds to the subtraction of the second term in U_{coh}.

When $\Gamma \gg 1$, the average values of U_{coh} are well approximated by the Madelung energy of the ground state Yukawa lattice which is either the bcc (for smaller

This document is provided by JAXA.

ξ) or the fcc (for larger ξ) lattice[17–19] with the relative difference of less than 0.01%. We have a simple approximate expression[10]

$$\frac{U_{coh}}{N_p k_B T_p} \approx a_1 \Gamma \exp(a_2 \xi) + a_3 \Gamma^{1/4} \exp(a_4 \xi) \tag{11}$$

with $a_1 = -0.896$, $a_2 = -0.588$, $a_3 = 0.72$, and $a_4 = -0.22$ which reproduces the cohesive energy within relative error less than 1% for $20 \leq \Gamma$ and $0 \leq \xi \leq 5$ (the coefficient $a_1 = -0.896$ is chosen so as to fit both bcc value $-0.89593\ldots$ and fcc value $-0.89587\ldots$ for $\xi = 0$).

We now take the finite size of particles into account, assuming that particles are hard spheres of radius r_p and the charge $-Qe$ is uniformly distributed on the surface. The potential around a particle is given for $r > r_p$, by[20,21]

$$\frac{(-Qe)}{1 + r_p/\lambda} \frac{\exp[-(r - r_p)/\lambda]}{r} = \frac{(-\tilde{Q}e)}{r} \exp(-r/\lambda), \tag{12}$$

where

$$\tilde{Q} = Q \frac{\exp(\tilde{r_p})}{1 + \tilde{r_p}} \tag{13}$$

and

$$\tilde{r_p} = \frac{r_p}{\lambda}. \tag{14}$$

The interaction between particles is then given by the DLVO potential which is still of the Yukawa type out of hard cores

$$\frac{(-\tilde{Q}e)^2}{r} \exp(-r/\lambda) \quad \text{for} \quad r > 2r_p, \tag{15}$$

r being the distance between centers.

In order to express the effect of hard cores of finite radius, we introduce another dimensionless parameter Γ_0 defined by

$$\Gamma_0 = \frac{(Qe)^2}{r_p k_B T_p} = \Gamma \frac{a}{r_p} \tag{16}$$

in addition to Γ and ξ. Values of $\tilde{r}_p$ is related to them as

$$\tilde{r}_p = \frac{r_p}{\lambda} = \frac{a}{\lambda} \frac{r_p}{a} = \xi \frac{\Gamma}{\Gamma_0}. \tag{17}$$

We also define $\tilde{\Gamma}$ by

$$\tilde{\Gamma} = \frac{(\tilde{Q}e)^2}{a k_B T_p} = \Gamma \frac{\exp(2\tilde{r}_p)}{(1 + \tilde{r}_p)^2}. \tag{18}$$

The Yukawa system with hard cores is thus characterized by a set of three dimensionless parameters, (Γ, ξ, Γ_0) or $(\tilde{\Gamma}, \xi, \tilde{r}_p)$. In terms of the latter, the energy associated with the sheath around a particle is written as

$$\frac{\tilde{U}_{sheath}}{N_p k_B T_p} = -\frac{1}{2} \tilde{\Gamma} \xi (1 + \tilde{r}_p) \exp(-2\tilde{r}_p). \tag{19}$$

The Coulombic part of the Helmholtz free energy of the system of particles is then given by

$$\begin{aligned} &\frac{F^{(p)} - F_{id}^{(p)}}{N_p k_B T_p} = f^{(p)}(\tilde{\Gamma}, \xi, \tilde{r}_p) \\ &\approx \int_0^{\tilde{\Gamma}} \frac{d\tilde{\Gamma}}{\tilde{\Gamma}} \frac{\tilde{U}_{coh} + \tilde{U}_{sheath}}{N_p k_B T_p} \\ &= a_1 \tilde{\Gamma} \exp(a_2 \xi) + 4 a_3 \tilde{\Gamma}^{1/4} \exp(a_4 \xi) \\ &+ \frac{3}{2} \tilde{\Gamma} \xi^{-2} [1 - (1 + 2\tilde{r}_p) \exp(-2\tilde{r}_p)] \\ &\quad - \frac{1}{2} \tilde{\Gamma} \xi (1 + \tilde{r}_p) \exp(-2\tilde{r}_p). \end{aligned} \tag{20}$$

For the equation of state given by the hard-sphere part $F_{id}^{(p)}$, we adopt the Carnahan-Stirling formula[22]. From these expressions, we have

$$\begin{aligned} &\frac{p_p}{n_p k_B T_p} \approx \frac{1 + \eta + \eta^2 - \eta^3}{(1 - \eta)^3} \\ &+ a_1 \tilde{\Gamma} e^{a_2 \xi} \left(\frac{1}{3} + \frac{1}{6} a_2 \xi + \frac{\tilde{r}_p^2}{1 + \tilde{r}_p} \right) \\ &+ a_3 \tilde{\Gamma}^{1/4} e^{a_4 \xi} \left(\frac{1}{3} + \frac{2}{3} a_4 \xi + \frac{\tilde{r}_p^2}{1 + \tilde{r}_p} \right) \\ &+ \frac{3}{2} \tilde{\Gamma} \xi^{-2} \frac{\tilde{r}_p^2}{1 + \tilde{r}_p} (1 + e^{-2\tilde{r}_p}) - \frac{1}{4} \tilde{\Gamma} \xi e^{-2\tilde{r}_p} \end{aligned} \tag{21}$$

and the expression for the inverse isothermal compressibility. Here

$$\eta = \left(\frac{r_p}{a} \right)^3 = \left(\frac{\Gamma}{\Gamma_0} \right)^3 \tag{22}$$

is the packing fraction.

The inverse isothermal compressibility can be negative with large absolute values when $\tilde{\Gamma} \gg 1$, the energy associated with the sheath (the fifth term) giving a significant contribution. As a property of the Yukawa OCP, the isothermal compressibility thus diverges at some critical value in the range[8,9] $1 < \tilde{\Gamma} < 10$. The analysis of thermodynamic behavior of the system in

This document is provided by JAXA.

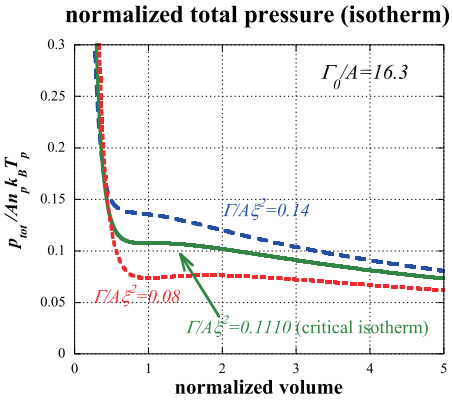

Fig. 3 Examples of the behavior of the total pressure along isotherms.

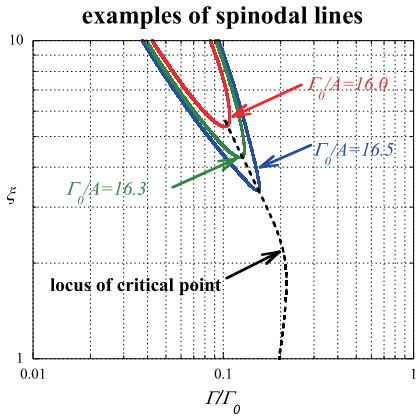

Fig. 4 Spinodal lines and locus of critical point (broken line).

total, however, we have to take the ambient microscopic particles into account whose densities are much larger than particles. Therefore, as is shown below, the effect of diverging compressibility of the Yukawa OCP appears as a property of total system only when $\tilde{\Gamma} \gg 1$ where our interpolation has sufficient accuracy.

Including the contribution of microscopic particles, we have the total pressure of the system p_{tot} approximately expressed as

$$\frac{p_{tot}}{n_p k_B T_p} \approx \frac{A}{1-\eta} + \frac{p_p}{n_p k_B T_p}. \tag{23}$$

Here

$$A = \frac{N_e k_B T_e + N_i k_B T_i}{N_p k_B T_p} \gg 1 \tag{24}$$

is the ratio of ideal gas contribution of microscopic particles to that of particles: The inequality comes from the assumption that the number densities of microscopic particles are much larger than macroscopic particles. We have taken the effect of the finite volume of particles as the reduction of free volume for microscopic particles in the form of the denominator of the first term of Eq. (23). The inverse isothermal compressibility of the system is thus given by

$$-\frac{V}{n_p k_B T_p}\left(\frac{\partial p_{tot}}{\partial V}\right)_{T_e,T_i,T_p} \approx \frac{A}{(1-\eta)^2} - \frac{V}{n_p k_B T_p}\left(\frac{\partial p_p}{\partial V}\right)_{T_e,T_i,T_p}. \tag{25}$$

For the thermodynamic instability of our system, the negative contribution to the inverse isothermal compressibility from strongly coupled particles has to overcome not only their own ideal gas contribution but also much larger positive contribution of background plasma. Therefore it is necessary to analyze the instability of the whole system and the background plasma plays an essential role in determining characteristic parameters for such a instability.

4. Thermodynamic instability and phase diagrams

Normalized total pressure of the system $p_{tot}/n_p k_B T_p$ is a function of parameters A, Γ, ξ, and Γ_0. Since usually $A \gg 1$, we have to be at least in the domain $\Gamma_0 > \Gamma \geq A \gg 1$ for the instability and Yukawa particles have to be very strongly coupled. When $\Gamma \gg 1$, $(p_{tot}/n_p k_B T_p)/A$ and $[-V(\partial p_{tot}/\partial V)_T/n_p k_B T_p]/A$, are approximately expressed as functions of $(\Gamma/A,\ \xi,\ \Gamma_0/A)$. Examples of p_{tot}-V isotherms are shown in Fig. 3. Some examples of the lines corresponding to the condition $(\partial p_{tot}/\partial V)_T/n_p k_B T_p = 0$ (spinodal lines) are shown in Fig. 4. The coexisting phases with the common pressure are determined by the usual Maxwell's rule[23]. Examples of resultant phase diagrams in the $(\Gamma,\ \xi)$-plane are shown in Fig. 5. The isotherm corresponds to lines $\xi \propto \Gamma^{1/2}$ in this plane and we have coexisting phases with different densities in the domain inside of phase separation lines. The phase diagrams expressed in terms of another set of variables, $(p_{tot},\ \Gamma/\xi^2)$, are shown in Fig. 6: This is the equivalent of the p-T diagram in the usual gas-liquid phase transition. The line giving coexisting phases ends at the critical point corresponding to the appearance of the extremum in the isotherms or the divergence in the isothermal compressibility. We have enhanced density fluctuations near the critical point[7,8].

This document is provided by JAXA.

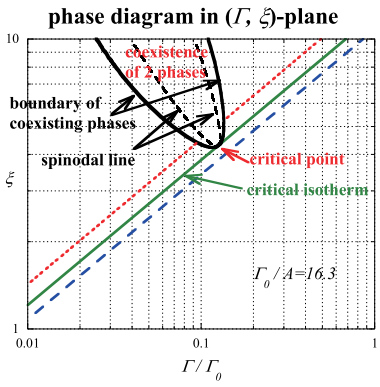

Fig. 5 An example of phase diagram. Inside the solid line, we have a phase separation and the broken line is the spinodal line.

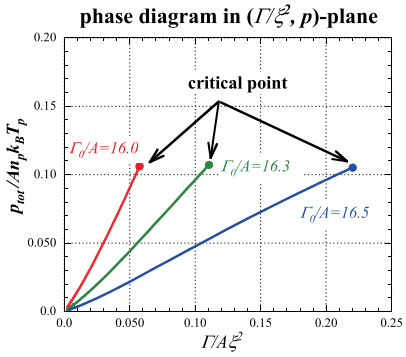

Fig. 6 Phase diagrams and critical points in $(p_{tot}, \Gamma/\xi^2)$-plane.

5. Density fluctuations

The density fluctuation spectrum is related to the dielectric response function via the fluctuation-dissipation theorem. On the other hand, at long wavelengths, the system responds to the perturbation by the compresibility. These relations (the compressibility sum rule) give the density fluctuation spectrum[10)]

$$S(k) \sim \left[-\frac{V}{n_p k_B T_p} \left(\frac{\partial p_{tot}}{\partial V} \right)_{T_i, T_e, T_p} + \mathscr{O}\left(k^2\right) \right]^{-1} \tag{26}$$

indicating the critical behavior of density fluctuations.

For OCP, on the other hand, the fluctuation-dissipation theorem gives the long-wavelength behavior of the structure factor in the form

$$S_{OCP}(k) \sim \left[k_D^2 \lambda^2 - \frac{V}{n_p k_B T_p} \left(\frac{\partial p_p}{\partial V} \right)_{T_p} + \mathscr{O}\left(k^2\right) \right]^{-1}, \tag{27}$$

where $k_D^2 = 4\pi n_p (Qe)^2 / k_B T_p$. (The pressure and the isothermal compressibility here are those of Yukawa OCP.) The vanishing of the inverse isothermal compressibility is not directly related to the enhancement of the density fluctuation. This relation has been derived for OCP's in a polarizing background and confirmed by a comparison with numerical simulations[24)]. In the case of $\lambda \to \infty$ (Coulombic OCP), we have the known result

$$S_{OCP}(k) \sim \left(\frac{k}{k_D} \right)^2 \left[1 - \frac{V}{n_p k_B T_p} \left(\frac{\partial p_p}{\partial V} \right)_{T_p} \left(\frac{k}{k_D} \right)^2 \right]^{-1}. \tag{28}$$

Part II: Experiments

6. Apparatus and experimental parameters

Experiments have been performed in the apparatus PK-3 PLUS, a plasma chamber filled with Ar gas and excited by the rf of 13.56 MHz through the parallel-plate-type electrodes[11)]. Fine particles of several diameters can be injected to the plasma. The diameters, the range of the pressure, and rf power are listed in table 1.

The images of fine particles are scanned by the CCD camera and converted into digital data of coordinates of particles. The velocity of particles is small enough, in comparison with the scanning speed, to give three-dimensional data. The number density of particles is obtained directly.

As for other physical parameters, values are not more than those expected under similar conditions. When one is interested only in the behavior of fine particles, the results of observations are clear. When one tries to relate them to theoretical predictions, however,

Table 1 Parameters in PK-3 Plus.

diameter of fine particles	1.55, 2.55, 3.42 μm
	6.81, 9.19, 14.92 μm
neutral gas	Ar, Ne
neutral gas pressure	5-255 Pa
rf power	0-4000 mW

This document is provided by JAXA.

Table 2 Assumed values of plasma parameters which are not directly measured.

ion density	$(1-10)\cdot 10^8 \mathrm{cm}^{-3}$
ion temperature	300 K
electron density	charge neutrality
electron temperature	(1-3) eV

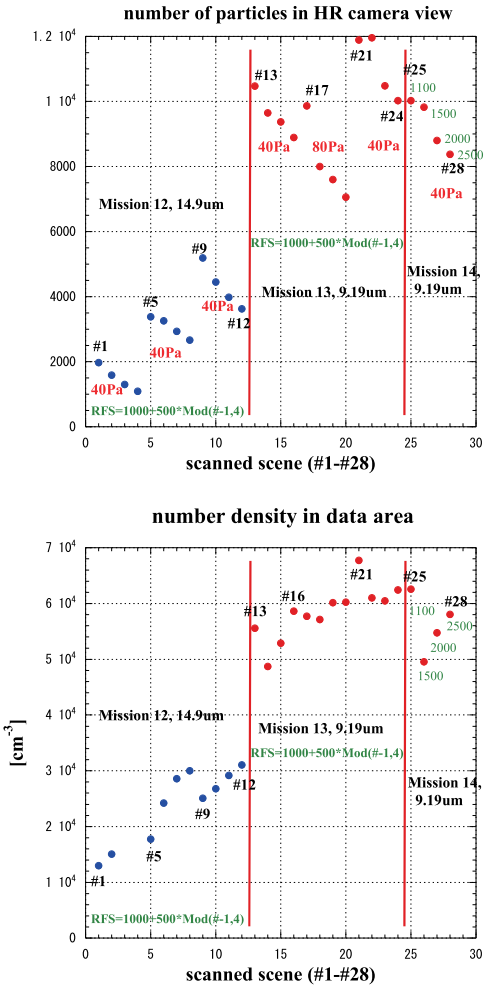

Fig. 7 Parameters of ISS experiments. The number of particles captured by the high resolution (HR) camera and the number density in the domain adopted for observation.

physical parameters not measured directly sometimes become important. In our case, physical parameters of the ambient plasma are mostly nothing more than those extrapolated from similar experiments. They are the electron density n_e, the ion density n_i, the electron temperature T_e, and the ion temperature T_i. We assume them as in Table 2.

To observe the critical point, strongly coupled states of fine particles are necessary. Since the parameter Γ is proportional to the square of the charge of particles, we need high density and high charges of particles. Such a state may be realized by frequent injections of larger particles and high power of rf excitations: Charges on a particle is approximately proportional to the radius and the electron temperature. Parameters for the apparatus, however, have not been well-established for these high density states and trials and errors have been inevitable. From Mission 11 to Mission 14, some sequences of experiments were assigned for our purpose.

In Fig. 7, we plot the number of particles captured by the CCD camera and the number density of particles in samples as function of the "scene" number or the serial number of samples. We observe that, the number and the number density increase with the of scene number. The dependence on the radius of particles has two aspects: Larger particles can have larger charges but also requires high rf excitation which induces larger void.

In order to compare the results with theoretical predictions, the characteristic parameters of experiments are plotted in the $\Gamma/\Gamma_0-\xi$-plane as shown in Fig. 8. (A preliminary report has been given[25].) Here, contours express the enhancement factor of the density fluctuations and the values of Γ/Γ_0 are directly obtained from the data of experiments. Those of $\xi = a/\lambda$, however, needs the ion density and ion temperature: The electron temperature is believed to be much higher than that of ions and λ is mostly determined by ions. Even if we assume that the ions are at the room temperature, the accurate information of the ion density is lacking and we have to assume that the ion density is $10^8 \sim 10^9$ cm^{-3}. The data points thus vertically move dependent on the ion density.

We observe that the characteristic parameters of experiments are approaching to expected critical point in later Missions. At the same time, we have to admit that they are still far from the target.

7. Structure factor

Let us remember some definitions and relations including the structure factor. The pair correlation function $g(r)-1$ is related to the structure factor $S(k)$ via

$$[g(\mathbf{r})-1] = \frac{1}{(2\pi)^3 n}\int d\mathbf{k}\exp(i\mathbf{k}\cdot\mathbf{r})[S(\mathbf{k})-1] \quad (29)$$

and

$$S(\mathbf{k})-1 = n\int d\mathbf{r}\exp(-i\mathbf{k}\cdot\mathbf{r})[g(\mathbf{r})-1]. \quad (30)$$

This document is provided by JAXA.

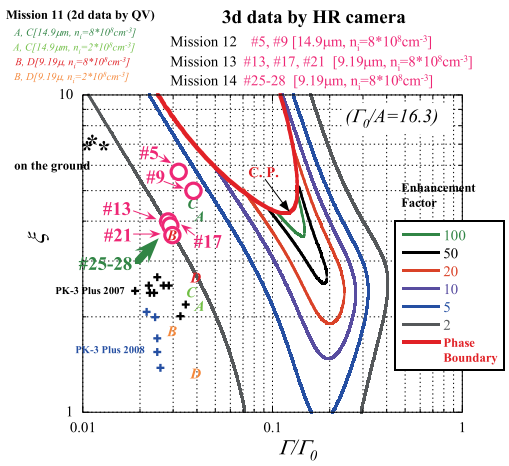

Fig. 8 Characteristic parameters of ISS experiments.

The structure factor is also expressed as

$$S(\mathbf{k}) = \frac{1}{N} < |\rho_{\mathbf{k}}|^2 >, \tag{31}$$

where

$$\rho_{\mathbf{k}} = \sum_{i=1}^{N} \exp(-i\mathbf{k}\cdot\mathbf{r}_i) \tag{32}$$

is called the density fluctuation, N is the total number of particles, and $< >$ denotes the statistical average. Since the computation of $S(\mathbf{k})$ via the Fourier transform of the pair correlation function in the real space does not give reliable result at long wavelengths, we have computed the structure factor directly by Eq. (31).

From three-dimensional distributions of particles, we select the domains as samples which include enough number of particles and, at the same time, are apparently homogeneous. We regard the distribution in the sample is repeated periodically all over the space. We take the average of their squared magnitude over all possible wave numbers within a small range of k, implicitly assuming the spherical symmetry. The size of the sample determines the smallest wave number as the argument of the structure factor.

When the rf power is raised, we have usually the void in the central part of the discharge. Since we have no particles in the domain of void, we have to take our samples from the domain surrounding the void. With the increase of the rf power, the domain of particles' existence becomes thinner and samples, smaller.

An example is shown in Fig. 9. We observe the enhancement of the fluctuation at long wavelengths. In order to confirm that the enhancement near $k = 0$ is not the effect of inhomogeneity, we artificially added such an inhomogeneity to the data of the Yukawa OCP obtained by numerical simulations and compared their effects with our observation. The results are also shown in Fig. 9. We see that, when the density is modified artificially by $\pm 10\%$ within the domain, the structure factor at $k \sim 0$ is enhanced. The extent of enhancement, however, seems to be smaller than what we have observed in experiments: *Though our data may not be*

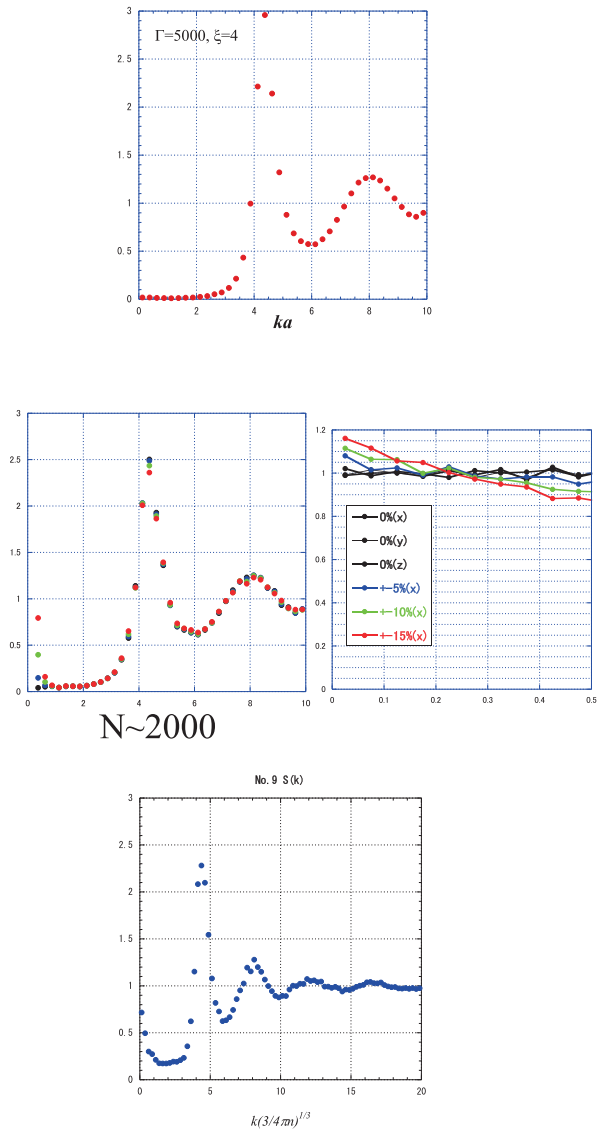

Fig. 9 Effect of artificially-introduced inhomogeneity of the system (middle right), modifying the original structure factor (top) to the one with enhanced fluctuations at long wavelengths (middle left), in comparison with observation (bottom).

This document is provided by JAXA.

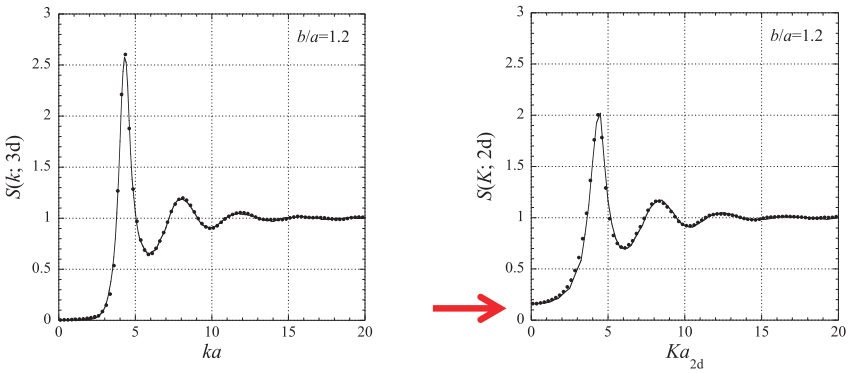

Fig. 10 The enhancement of density fluctuations due to reduction of dimensions (sample size). When three-dimensional sample is sliced into slabs, the original three-dimensional structure factor (left) is observed as the one accompanying the enhanced fluctuations at long but not so long wavelengths (right).

without the effect of inhomogeneity of the system, results obtained by experiments seem to be beyond those effects.

The enhancement of the structure factor in the domain $ka \ll 1$ but not $ka \sim 0$ may attributed to the effect of finiteness of the observed system. In the case where we observe a three-dimensional system through nearly two-dimensional window, we have similar enhancement of the fluctuations[26]. An example is given in Fig. 10. The three-dimensional system is sliced into two-dimensional systems and the three-dimensional coordinates are projected onto a two-dimensional plane. In this process, the fluctuations in the density are enhanced. By the inverse conversion, we are able to recover the original behavior of the structure factor. When we observe a finite domain including large but finite number of particles, we have similar enhancement of fluctuations. We expect to be able to restore the original structure factor which would be observed when we have large enough window. Investigation in this direction is in progress.

8. Conclusions

In order to realize the physical parameters of fine particle plasma corresponding to the possible critical point, high densities with large fine particles are necessary. For high density states, heavy injections and high power of rf excitation are needed. These states have been tried in PK-3 PLUS.

With the increase of the rf power, the void appears in the central part of the plasma. When we have voids, the domain of fine particles is restricted in a relatively narrow region. The domain where particle distribution is homogeneous becomes smaller due to the appearance of voids.

Characteristic parameters have been estimated based on the direct information obtained from observations and also from expectations. Though they have approached to the critical point in the course of experiments, they are still not close to the point.

The structure factor observed in experiments shows the enhancement at long wavelengths. Compared with the effects due to the inhomogeneity of the system which is artificially added, the observed enhancements seem to be larger than expected from those effects. Though we are still not close to the critical point and our data suffer from the effects of inhomogeneity and smallness of samples, the enhancement of the long wavelength fluctuations seems to have been observed. When we are able to have fine particles plasmas without void, closer observations of the critical behavior will be possible.

Acknowledgments

The authors would like to thank members of the research group at Max-Planck Institute for Extraterrestrial Physics lead by Professor G. E. Morfill and the research group at the Joint Institute for High Temperatures lead by Professor V. E. Fortov for kind cooperation throughout this work. They also thank the ISS Science Project Office for financial support.

References

1) Shukla, P. K. and Mamun, A. A., *Introduction to Dusty Plasma Physics*, Inst. Phys., London, 2002.

This document is provided by JAXA.

2) Fortov, V. E., Ivlev, A. V., Khrapak, S. A., Khrapak, A. G., and Morfill, G. E., Phys. Rep., Vol. 421, (2005), pp. 1–103.
3) Tsytovich, V. N., Morfill, G. E., Vladimirov, S. V., and Thomas, H., *Elementary Physics of Complex Plasmas*, Springer, Berlin, 2008.
4) Morfill, G. E. and Ivlev, A. V., Rev. Mod. Phys., Vol. 81, (2009), pp. 1353–1404.
5) Khrapak, S, Morfill, G. E., Ivlev, A. V., Thomas, H. M., Beysens, D. A., Zappoli, B., Fortov, V. E., Lipaev, A. M., and Molotkov, V. I., Phys. Rev. Lett., Vol. 98, (2007), 095003.
6) Avinash, K., Phys. Rev. Lett., Vol. 96, (2006), 015001.
7) Totsuji, H. and Ichimaru, S., Prog. Theor. Phys. Kyoto, Vol. 52, (1974), pp. 42–53.
8) H. Totsuji, Totsuji, H., J. Phys. A: Math. Gen., Vol. 39, (2006), pp. 4565–4569.
9) Totsuji, H., *Non-Neutral Plasma Physics VI, Workshop on Non-Neutral Plasmas 2006*, ed. Drewsen, M., Uggerhøj, and Knudsen, H., AIP Conf. Proc., Vol. 862 (American Inst. Phys., New York, 2006), pp. 248–256.
10) Totsuji, H., Phys. Plasmas, Vol. 15, (2008), 072111.
11) Thomas, H. M., Morfill, G. E., Fortov, V. E. *et al.*, New J. Phys., Vol. 10, (2008), 033036.
12) For example, Pines, D. and Noziéres, P., *The Theory of Quantum Liquids, Vol. I: Normal Liquids*, W. A. Benjamin, New York, 1966, Chap. 3, p. 161.
13) For example, Landau, L. D. and Lifshitz, E. M., *Statistical Physics, 3rd Edition, Part I*, Pergamon, Oxford, 1988, Sect. 31.
14) For example, Baus, M. and Hansen, J.-P., Phys. Rep., Vol. 59, (1980), pp. 1–94.; March, N. H. and Tosi, M. P., *Coulomb Liquids*, Academic Press, London, 1984, Chap. 4.
15) Hamaguchi, S. and Farouki, R. T., J. Chem. Phys., Vol. 101, (1984), pp. 9876–9884.
16) Rosenfeld, Y., Phys. Rev. E, Vol. 49, (1994), pp. 4425–4429.
17) For example, Robbins, M. O., Kremer, K., and Grest, G. S., J. Chem. Phys., Vol. 88, (1988), pp. 3286–3312, and references therein.
18) Farouki, R. T. and Hamaguchi, S., J. Chem. Phys., Vol. 101, (1994), pp. 9885–9893.
19) Hamaguchi, S, Farouki, R. T., and Dubin, D. H. E., Phys. Rev. E, Vol. 56, (1997), pp. 4671–4682.
20) Deryagin, B. and Landau, L., Acta Phys. -Chim. USSR, Vol. 14, (1941), pp. 633–662.
21) Verwey, E. J. W. and Overbeek, J. Th. G., *Theory of the Stability of Lyophobic Colloids*, Elsevier, New York, 1948.
22) Carnahan, N. F. and Stirling, K. E., J. Chem. Phys., Vol. 51, (1969), pp. 635–636.
23) For example, Landau, L. D. and Lifshitz, E. M., *Statistical Physics, 3rd Edition, Part I*, Pergamon, Oxford, 1988, Sect. 84.
24) Totsuji, H. and Tokami, K., Phys. Rev. A, Vol. 30, (1984), pp. 3175–3182.
25) Totsuji, H., Takahashi, K., Adachi, S., Hayashi, Y., and Takayanagi, M., J. Jpn. Soc. Microgravity Appl., Vol. 28, (2011), pp. S27–S30.
26) Totsuji, H, J. Phys. Soc. Jpn., Vol. 78, (2009), 065004; Totsuji, H., J. Phys. Soc. Jpn., Vol. 79, (2010), 064002; Totsuji, H. and Totsuji, C., Phys. Rev. E, Vol. 85, (2012), 031139.

This document is provided by JAXA.